

Article

Reliability Analysis of Dynamic Sealing Performance in the Radial Hydraulic Drilling Technique

Lin Chai ¹ , Yongsheng Liu ^{2,*} , Guoqiang Chen ², Qiang Sun ¹, Wenlong Gao ³ and Zijun Dou ²

¹ Research Institute of Petroleum Exploration & Development, China National Petroleum Corporation (CNPC), Beijing 100083, China; linchai@petrochina.com.cn (L.C.); sun_yuppy@petrochina.com.cn (Q.S.)

² Department of Engineering Technology, China University of Geosciences (Beijing), Beijing 100083, China; 2102190060@cugb.edu.cn (G.C.); dzj3002220026@163.com (Z.D.)

³ Engineering Technology Research Institute, China National Petroleum Corporation Great Wall Drilling Engineering Co., Ltd., Panjin 124000, China; gqc.gwdc@cnpc.com.cn

* Correspondence: yongsheng@cugb.edu.cn

Abstract: Traditional coiled tubing radial drilling with the same diameter cannot support deep and ultra-deep wells for high-pressure hydraulic jet drilling due to small diameter and sizeable hydraulic loss over long distances. The novel downhole movable pipe radial hydraulic drilling technique extracts a small diameter high-pressure injection pipe from the (tubing pipe) oil pipe and then drills it horizontally into the formation to form a radial hole. Dynamic sealing is the core of this technology, which achieves high-pressure fluid sealing while ensuring the injection pipe smoothly slides out of the oil pipe. A sealing tool is designed between the tubing and the injection pipe to prevent the leakage of high-pressure fluid. In this paper, the finite element model of the sealing tool was established, and the deformation and stress of the sealing tool under different interference and fluid pressure were simulated and analyzed. The relationship between stress distribution and contact pressure under the corresponding conditions was obtained. The results show that the von Mises stress increases significantly with the increase in fluid pressure under certain interference conditions. When the fluid pressure was 35 MPa, 52 MPa, and 70 MPa, the maximum von Mises stress was 29.65 MPa, 30.87 MPa, and 32.47 MPa, respectively, within a reasonable range. The stress peak area changes simultaneously, indicating that the possible damage location changes with the fluid pressure change. The maximum contact pressure between the sealing ring and the smooth rod increases with interference and fluid pressure, which always meets the sealing conditions. A laboratory test bench was built to test the high-pressure sealing performance of the sealing tool. Combined with the simulation data and test results, the downhole continuous rod dynamic sealing tool was modified to provide theoretical guidance for practical application.

Keywords: dynamic seal; finite element analysis; contact pressure; HTHP



Citation: Chai, L.; Liu, Y.; Chen, G.; Sun, Q.; Gao, W.; Dou, Z. Reliability Analysis of Dynamic Sealing Performance in the Radial Hydraulic Drilling Technique. *Processes* **2024**, *12*, 807. <https://doi.org/10.3390/pr12040807>

Academic Editor: Qingbang Meng

Received: 19 March 2024

Revised: 14 April 2024

Accepted: 15 April 2024

Published: 17 April 2024



Copyright: © 2024 by the authors. Licensee MDPI, Basel, Switzerland. This article is an open access article distributed under the terms and conditions of the Creative Commons Attribution (CC BY) license (<https://creativecommons.org/licenses/by/4.0/>).

1. Introduction

The hydraulic radial drilling technology involves two processes, namely casing windowing and bottom drilling, the principle of which is to make a hole in the casing of the oil layer first, and then break strata with the help of the hydraulic jet action of a high-pressure jet and the rotating crushing action of a tiny drill bit, to form radial horizontal drilling. It is the product of the deep development of conventional horizontal well technology and the extension and expansion of horizontal well technology [1–5]. The radial hole with a small diameter perpendicular to the casing can be directly drilled into the oil and gas well reservoir. Multilayer radial horizontal holes can be drilled in different layers, making it an effective communication channel in fracture–cavity carbonate reservoirs, providing a gravity oil drainage method, expanding drainage area, and improving horizontal and vertical oil displacement efficiency. It also helps to achieve multi-target and three-dimensional production in one well, enhance the recovery of low permeability reservoirs, and reduce the

total cost of oil block recovery. At the same time, as an alternative to traditional perforation technology, the hydraulic radial drilling technology provides access to deeper oil and gas channels, while avoiding damaging the formation, casing, and cement ring and reducing the likelihood of drilling accidents [6–10]. So far, this technology has been extensively applied worldwide, and many companies in China have introduced foreign technologies for the application of radial drilling technology in various oil fields and achieved a certain amount of progress.

To significantly improve the utilization of reserves, it is necessary to achieve all-around communication using hydraulic jet radial drilling and well completion technology, as there are many fractures and holes near the wellbore in the Tahe ultra-deep (5500–6500 m) carbonate reservoir. Compared with the eastern clastic rocks, Tahe limestone has the characteristics of higher hardness, greater depth, higher temperature, and higher pressure, with a higher requirement on the energy of drilling holes by hydraulic jet [11–13]. The existing traditional hose-type hydraulic jet radial drilling technology (as shown in Figure 1) makes it challenging to meet the construction requirements. Due to the small diameter of the coiled tubing and significant water energy loss along the pipeline, the practical work used for rock breaking needs to be improved. Moreover, low construction displacement is unfavorable to drilling cuttings return and limits operating depth (generally applicable to wells with a depth of less than 3500 m). At the same time, deep well operation is accompanied by the potential risk of wellhead high-pressure hose.

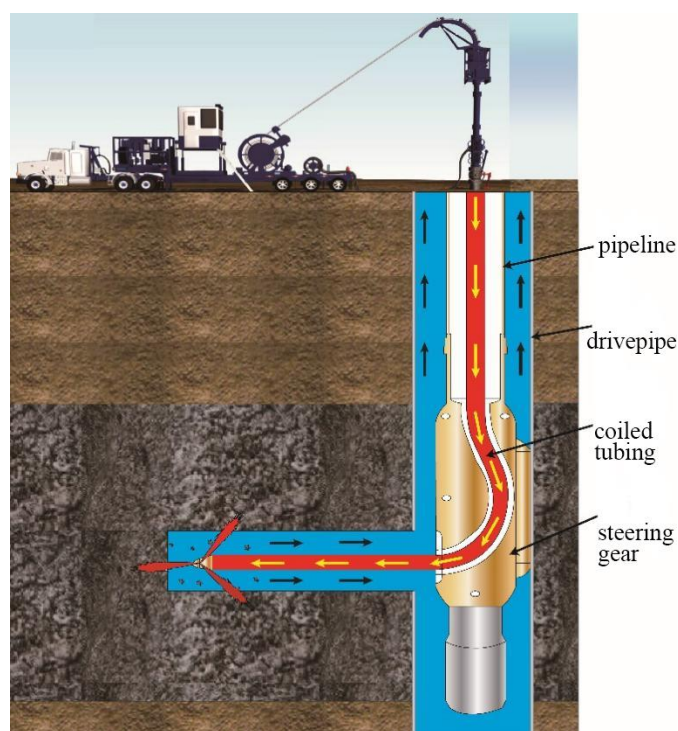


Figure 1. Coiled tubing radial hydraulic drilling technology.

PetroJet, a Canadian company, innovatively proposed a novel downhole movable pipe radial hydraulic drilling technique (as shown in Figure 2). The core of the drilling process is to run a continuous pumping rod through the tubing and inject fluid through the tubing and the annulus of the continuous pumping rod. The fluid enters the drill bit through the circulation device, forming a high-pressure hydraulic injection. After drilling, the fluid returns to the ground from the ring space between the oil pipe and the casing. The pumping rod is connected to the tubing into formation and pressurized to ensure that it passes through the dynamic seal at the lower end of the tubing for continuous feed in the horizontal borehole. The technology can significantly increase construction displacement,

reduce pipeline water loss, and improve rock-breaking and pore-forming efficiency. More importantly, it is expected to solve the problem of radial horizontal construction in deep and ultra-deep wells [14–19]. The novel downhole movable pipe radial hydraulic drilling technique is far from mature mainly because no achievements have been made in the key technology of dynamic seal assembly. Considering the actual conditions of the formation temperature and pressure changes, the requirements for sealing tools in underground equipment differ from those on the ground. Currently, the existing sealing tools can not meet the requirements of ultra-deep wells, mainly due to problems such as a too-small sealing gap, high sealing surface finish, and inability to achieve late insertion. PetroJet Company has carried out a pilot test. However, this technology is still in its initial research and development stage in China, without significant progress.

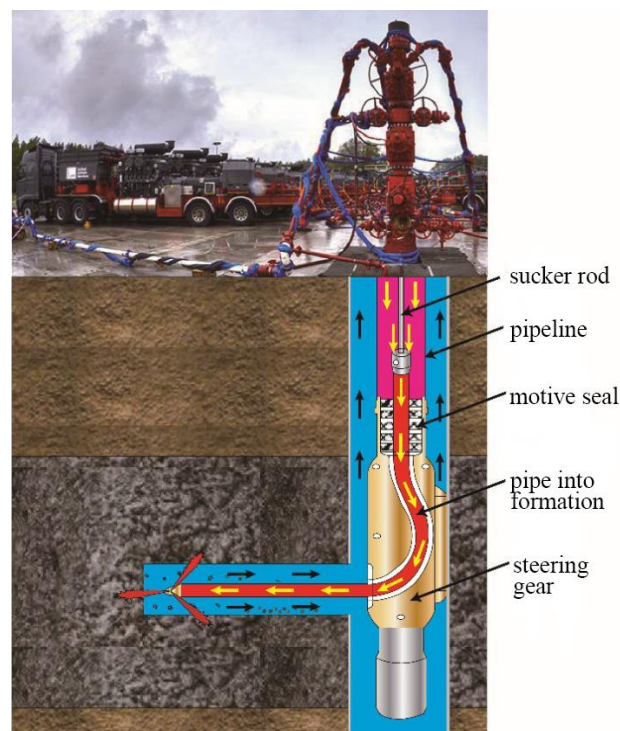


Figure 2. Downhole movable pipe radial hydraulic drilling technology.

In recent years, many domestic scholars have begun to conduct finite element simulation research on the sealing performance of sealing tools, with the research object being mostly elastomer rubber rings used for static sealing. Little research progress has been made in the simulation of high-pressure sealing tools in a radial horizontal well because of the special material characteristics of the sealing parts and harsh working conditions. In the existing literature, researchers have only analyzed the deformation and stress of seals under low oil pressure (≤ 7 MPa), while in modern hydraulic machinery, the oil pressure is generally above 15 MPa [20]. Due to the complex nonlinearity of rubber deformation and the existence of contact problems, the finite element software calculation makes it difficult to achieve convergence under high pressure, making it difficult to obtain correct results. In this paper, the critical structure of dynamic seals in the process of radial drilling with fixed hydraulic jets at the wellhead was designed, processed, and trial-produced, and the deformation and stress under medium and high-pressure conditions were simulated. Additionally, an indoor testbed was built to test the high-pressure sealing performance of the sealing tool, which provides a scientific theoretical basis for the optimal design of sealing structures to realize the smooth downhole operation of the dynamic seal component and meet the requirements for the tool's performance.

2. Dynamic Seal Structure

The sealing structure, an essential working element in the novel downhole movable pipe radial hydraulic drilling technique, plays a sealing role by pre-tightening force generated by extrusion deformation. The sealing tool and the injection pipe should not be held too tightly. Otherwise, the sealing components will be severely worn, affecting the sealing effect and the operation of the continuous pumping rod. There should be no clearance between the seal and the injection pipe, which will affect the formation of an effective initial seal between them. The seal shall not be removed from its position before it is inserted. The failure of the seal leads to leakage of high-pressure fluid, making the jet pipe incapable of obtaining high-pressure fluid and thus affecting drilling in the radial well. Based on the above requirements, a continuous smooth rod sealing tool was devised after comprehensively investigating the sealing materials and forms. To better analyze the sealing performance, it is important to establish a model and select proper sealing materials. The structure in which the triangular sealing component is located between two centralizing ring groups is adopted for the dynamic seal design scheme (Figure 3). The structural design of the dynamic seal is shown in Figure 4 [21–24]. The upper and lower centralizing rings play an important role in centralizing the continuous pumping rod, ensuring a good sealing effect while preventing the pumping rod from being stuck because of too small gaps. The sealing casing comprises an upper joint, a centralizing sleeve, a center barrel, and a lower joint. The sealing components of the tool are between the O-ring and the sealing chamber and between the triangular seal and the continuous pumping rod. With excellent extrusion and wear resistance, the triangular seal applies to cases with significant gaps and, thus, has become the optimal rubber contact dynamic sealing material. The narrow contact area improves the sealing effect and reduces friction.

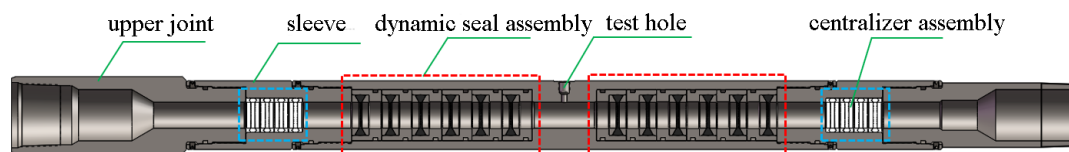


Figure 3. Dynamic seal structure profile.

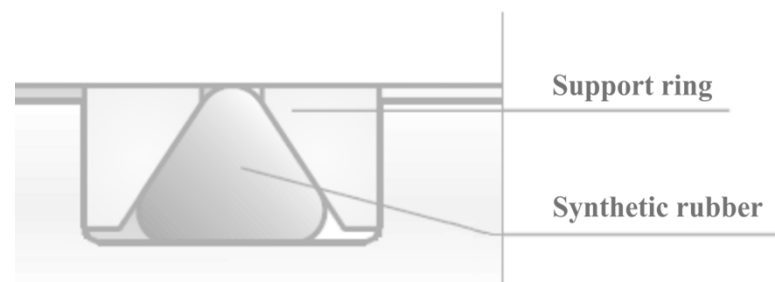


Figure 4. Structural diagram of triangular seal.

3. Numerical Simulation of Sealing Performance

3.1. Finite Element Model

Considering that boundary conditions were complex and the sealing casing had no influence on the sealing of rubber material, the components of the seal casing were combined for analysis. In the assembly of the sealing tool, the rubber material repressed the surface tightly because of its elastic deformation ability, creating a self-pressurized initial seal at low pressure. After entering the working fluid, the fluid pressure squeezed and pressed the sealing rings tightly on the sealing surfaces, thus achieving encapsulation and avoiding fluid leakage through the gap. The higher the working pressure, the greater the pressing force. The analysis of the sealing structure was simplified without affecting the accuracy of finite element analysis. The force and deformation were distributed axisymmetrically as smooth rod sealing tool components are all rotatory and completely axisymmetrically.

installed. Therefore, a two-dimensional axisymmetric model is established by taking the cross-section [25–27], and a three-dimensional simulation model is generated using the imaging principle.

In general, the amount of compression of the seal refers to the amount of compression caused by the extrusion of the seal after installation. The different compression amounts of the seal will change the contact pressure, contact width, and friction force between the seal and the sealed part during the working process. The triangular sealing interference amount (δ) directly affects the setting of the inner tube and the initial sealing effect. The sealing performance of the sealing tool was detected by entering the high-pressure fluid under different pressures [28]. Therefore, the sealing performance was improved by controlling the seal's interference. According to the above definition of compression amount, the seal can work under different compression amounts by adjusting the diameter D of the triangular sealing ring, as shown in Figure 5. Therefore, in the following part, the interference amount (δ) and the fluid pressure are taken as parameters (Figure 6), with the former being 0.25 mm, 0.5 mm, and 0.75 mm, respectively, and the latter being 35 MPa, 52 MPa, and 70 MPa, respectively.

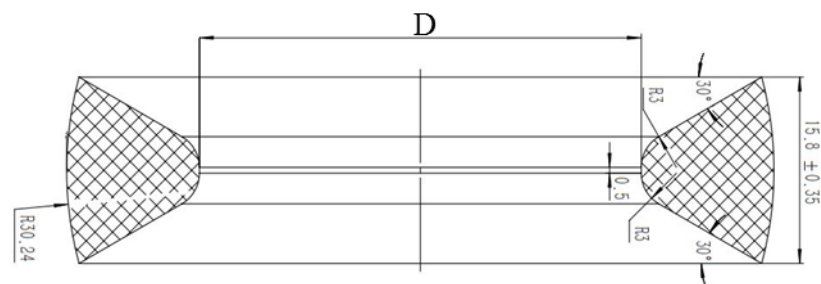


Figure 5. Structural diagram of rubber barrel.

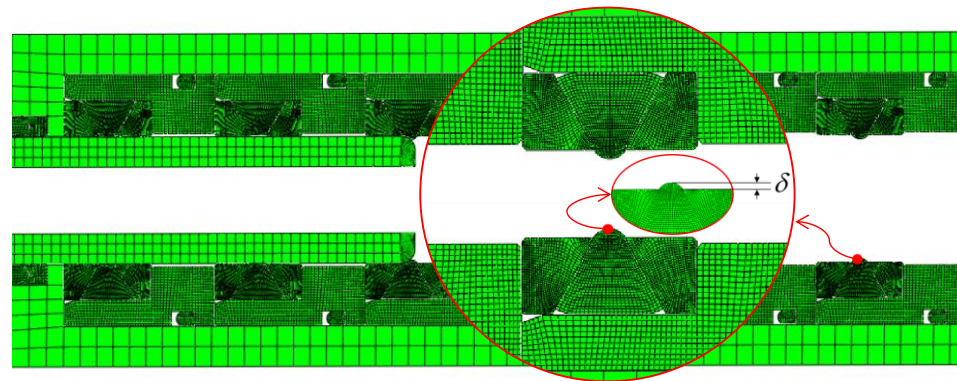


Figure 6. Finite element model of dynamic seal structure.

This study established the finite element calculation model of continuous smooth rod sealing tool using modern advanced finite element analysis software and making reasonable assumptions and pretreatment. The finite element method simulated the sealing tool's characteristics under various working conditions by calculating and analyzing the influence of multiple factors on the force and sealing characteristics of the triangular and O-ring seals. The following assumptions were made:

- (1) The material had definite elastic modulus and Poisson's ratio;
- (2) The material was continuous and uniform, the creep properties of tension and compression were the same, and the creep did not change volume [29];
- (3) The displacement of the smooth rod caused the compression of the triangular seal;
- (4) The smooth rod, whose elastic modulus was more significant than rubber material, was analyzed as a rigid body.

The commonly used sealing material is a typical hyperelastic material, anisotropic, highly deformable, highly elastic, and almost incompressible with elastic properties similar to metal materials and energy absorption properties similar to viscous liquids [30]. Poly-ether-ether-ketone (PEEK) was used to centralize ring groups. It is a special polymer material with a melting point of 334 °C, a softening point of 168 °C, and tensile strength of 132–148 MPa and has the advantages of high-temperature resistance, good self-lubrication, peeling resistance, and super mechanical properties, which can effectively prevent the surface of the continuous tube from being ground. Hydrogenated nitrile rubber (HNBR) was adopted for triangular sealers, as it has excellent temperature resistance, high strength, high tear performance, and excellent wear resistance. It is one of the rubbers with excellent comprehensive performance. By fitting the experimental data, C10 and C01 of HNBR were -5.928 and 18.54 , respectively, which were taken as the parameters of the constitutive relationship model. The physical parameters of the material are shown in Table 1.

Table 1. Physical parameters of materials.

Material	Density (g/mm ³)	Elastic Modulus (MPa)	Poisson's Ratio
G4140	7.83×10^9	200,000	0.29
PEEK	1.304×10^9	4600	0.38
NHBR	1×10^9	—	—

Nonlinear changes in material and geometry have an essential effect on sealing. There are some problems in practical application, such as complex boundary conditions and contact nonlinearity. The constitutive model and parameters have a significant influence on the analysis results. The Mooney–Rivlin model was adopted to characterize its characteristics in the simulation model, and its strain energy function is expressed as

$$W(I1, I2) = C10(I1 - 3) + C01(I2 - 3)$$

W—strain energy density function;

C10, C01—mechanical property constants of hyperelastic materials;

I1, I2—first and second invariant of right Cauchy–Green Deformation Tensor.

3.2. Boundary Conditions and Loading

First, the high-pressure injection pipe was moved up a certain distance to avoid contact with the triangular sealing parts. Second, it was displaced downward to a certain extent and the triangular seal was squeezed until it was deformed. Finally, pressure was applied to the fluid to reach its final contact deformation state. The high-pressure injection pipe was set as a rigid body without considering its deformation because of its high stiffness. The friction coefficient between rubber material and steel body was defined as 0.4 and between rigid bodies, it was 0.2. The penalty function method was adopted for each contact pair.

The whole moving process was divided into eight analytical steps. In the first analysis step, the interference assembly employed an automatic contraction fit, and the contact static pressure during assembly was simulated and analyzed. In the second step, the injection pipe was displaced along the Y axis and the rubber barrels were extruded individually. In the last six analysis steps, high-pressure fluid pressurized the seals individually. As shown in Figure 7, the three nodes of Unit 1 and Unit 2 are numbered 101, 102, and 103. The two corresponding units on the master surface are named 4 and 5, and the nodes from left to right are 201, 202, and 203. Firstly, 201 and 101, which are in contact with the fluid pressure from the master surface at the initial time, are defined as the starting points. The pressure penetration load will be loaded along these two points towards the contact point so that the node can be automatically adjusted with the deformation of the contact body and the change of the contact pressure. For nodes where the contact pressure is less than the critical contact pressure, the pressure is applied to the node until the contact pressure at a certain point is greater than the critical osmotic pressure. The fluid pressure loading

node automatically adjusts with the deformation of the contact body and the change of the contact pressure, which can accurately simulate the deformation process of the seal under the action of high-pressure fluid.

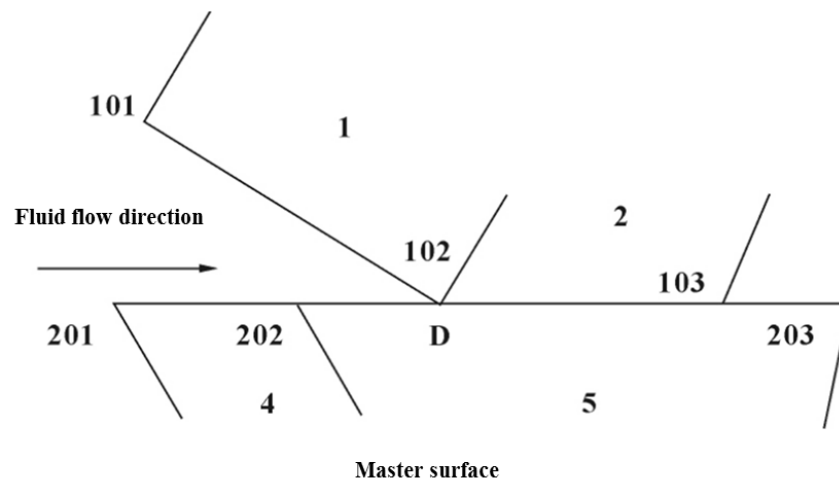


Figure 7. Application of fluid pressure penetration load.

All the structures in the finite element analysis model of the sealing tool adopt the four-node bilinear axisymmetric quadrilateral CAX4RH element to better simulate the large deformation and strain of hydrogenated NBR. To prevent leakage of high-pressure fluid, a sealing tool was designed to seal between the tubing and the injection pipe. The sealing parts were an O-ring and a triangular sealing ring made of hydrogenated nitrile rubber. Based on rubber's large deformation and strain, the finite element model was fine-meshed in some particular areas [28,31]. The finite slip is defined as the contact between the rubber cylinder and the pipe wall, and the boundary condition when the seal casing is completely fixed is defined. The analysis results were converged by refining the mesh locally, and the whole finite element model was finally established.

The number of grids has a crucial influence on the solution process. Too few grids will affect the accuracy and precision of the simulation results, and too many grids will increase the calculation amount. For parts of the shell that are not the focus of attention, a relatively thick mesh can effectively reduce the time of the analysis. Therefore, only the mesh-independent verification of the triangular sealing structure is carried out. When the interference amount (δ) is 0.50 mm, and the fluid pressure is 52 MPa, the maximum contact pressure of different mesh division results is shown in Figure 8.

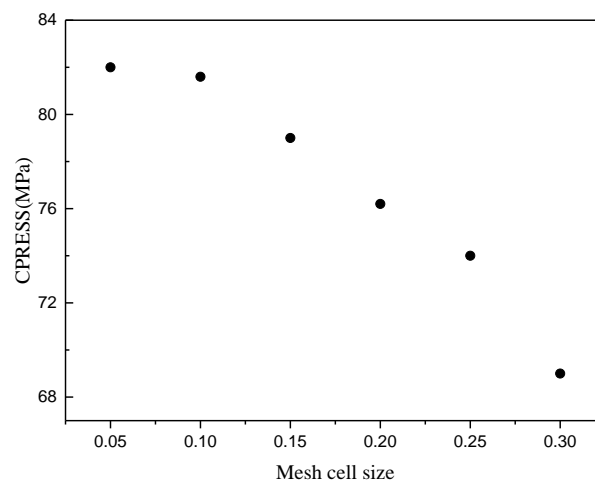


Figure 8. Mesh-independent verification.

When the mesh cell size is reduced to 0.1, the maximum contact pressure can be considered independent of the mesh. Finally, the mesh cell size of the triangular sealing structure is determined to be 0.1, and further calculation and analysis are carried out, as shown in Figure 9.

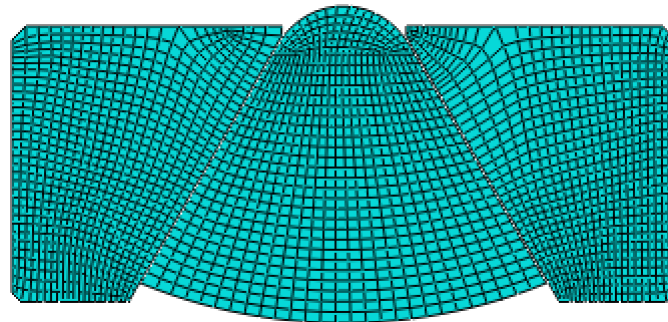


Figure 9. Finite element model of triangular sealing structure.

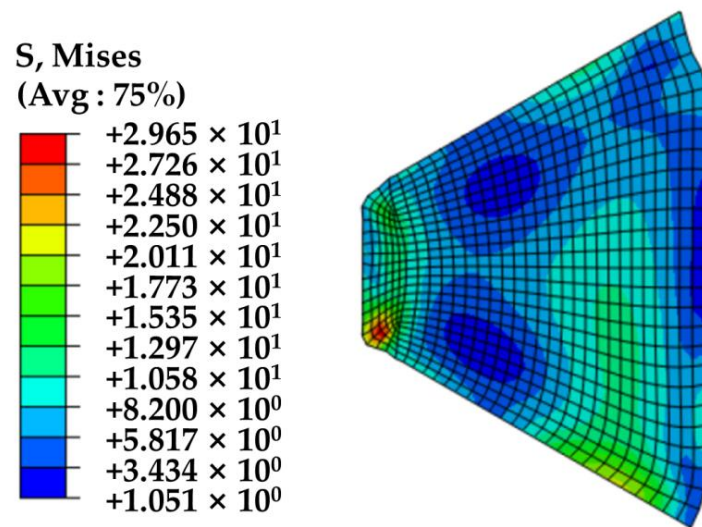
3.3. Analysis of Numerical Results

To evaluate the performance of the triangular seal, it is necessary to analyze the stress state of the rubber ring and the contact pressure at the sealing point as they are the main criteria to determine the life of the rubber ring and whether the rubber ring leaks. The research shows that the main causes of seal failure are tear leakage and less contact pressure than fluid pressure. There were two failure criteria for sealing in the simulation calculation setting [32–35].

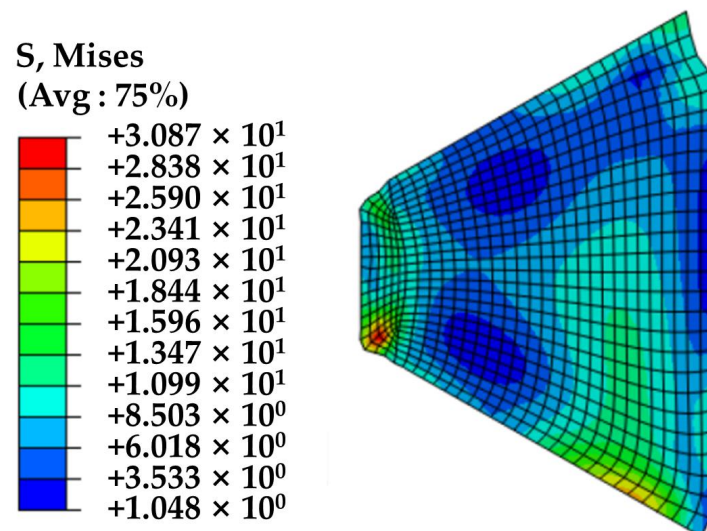
- (1) Maximum shear stress: When the seal was subjected to a certain amount of compression and the shear force was more significant than the shear strength, the sealing ring would crack, resulting in shear failure.
- (2) Maximum contact stress: When the contact stress between the seal and both sides of the contact surface was greater than the pressure value of the fluid, the sealing medium could be realized. Otherwise, leakage would occur, resulting in sealing failure.

The results indicated that the maximum von Mises stress and maximum contact stress of triangular and O-ring seals varied with the interference size and fluid pressure. Generally speaking, the larger the stress value is, the more prone the material is to crack, resulting in sealing failure [36]. In addition, the increase in stress would accelerate the relaxation of the rubber material, resulting in a decrease in “stiffness”. The magnitude and distributing rule of contact pressure reflects the strength of sealing ability. The distributed pressure is conducive to improving sealing ability, and the greater the equivalent pressure value, the stronger the sealing ability. The necessary sealing condition is that the maximum contact pressure on the sealing interface is greater than or equal to the fluid pressure.

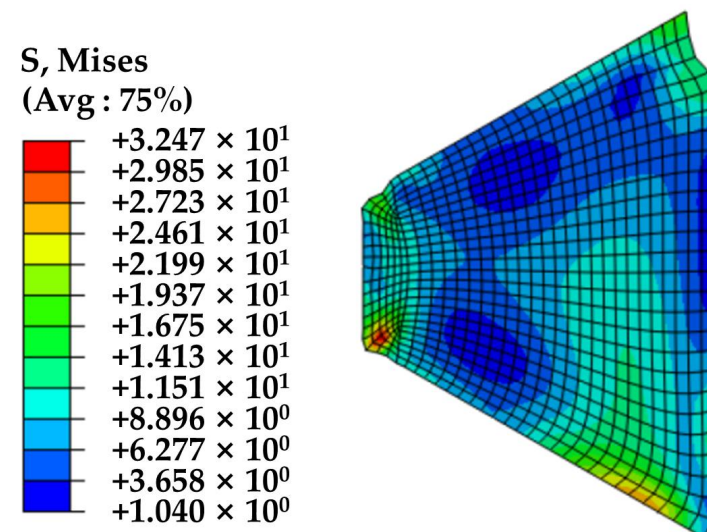
As can be seen from Figure 10, with a certain amount of interference, the von Mises stress on the rubber barrel significantly increased with the increase in fluid flow, with its maximum value of 29.65 MPa, 30.87 MPa, and 32.47 MPa under the fluid pressure of 35 MPa, 52 MPa, and 70 MPa, respectively. At the same time, the position of von Mises’s stress peak region changed with the increase in fluid pressure, which indicated that the possibility of failure of the rubber barrel increased under high-pressure fluid (Figure 11). The location where the cracks were most likely to occur also changed. The maximum von Mises stress under different fluid pressure and compression rates is shown in Table 2.



(a)

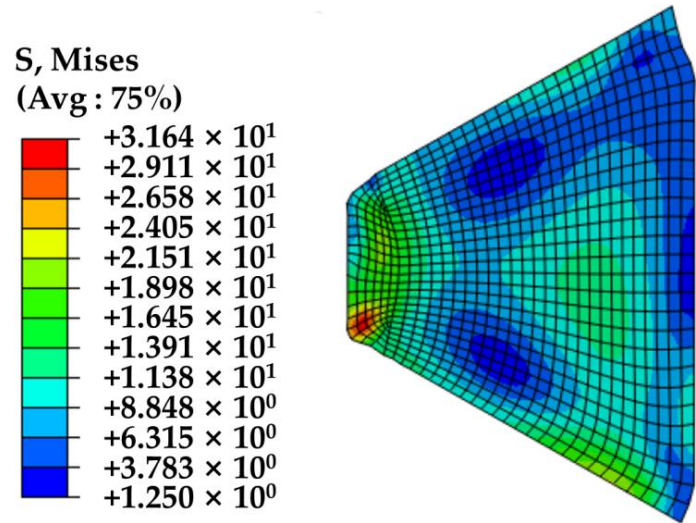


(b)

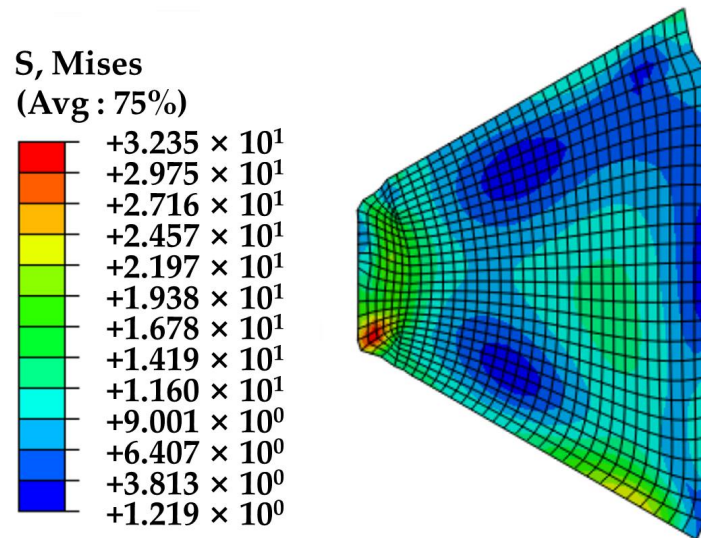


(c)

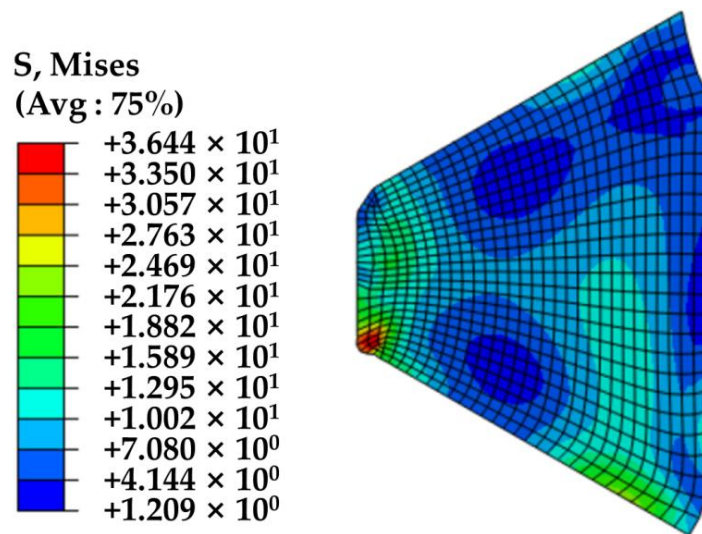
Figure 10. Cont.



(d)



(e)



(f)

Figure 10. Cont.

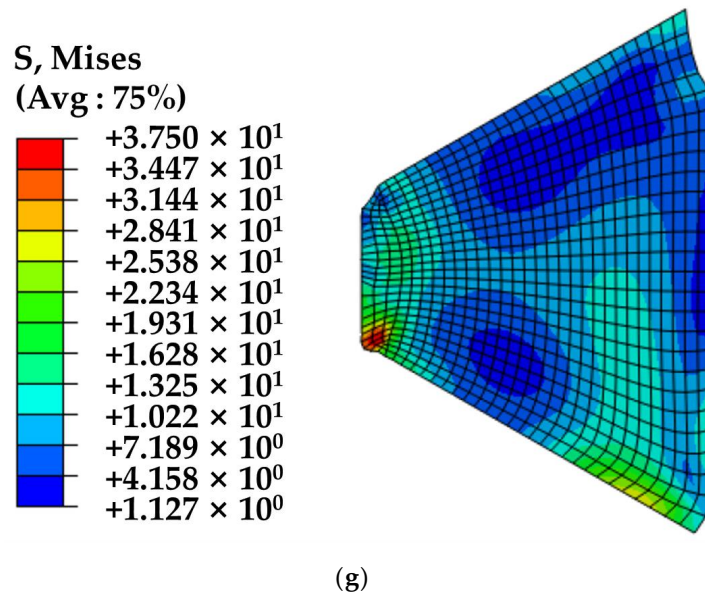


Figure 10. von Mises distribution figure under different fluid pressure and different amounts of interference: (a) diagram of stress distribution with interference of 0.25 mm and fluid pressure of 35 MPa; (b) diagram of stress distribution with interference of 0.25 mm and fluid pressure of 52 MPa; (c) diagram of stress distribution with interference of 0.25 mm and fluid pressure of 70 MPa; (d) diagram of stress distribution with interference of 0.5 mm and fluid pressure of 35 MPa; (e) diagram of stress distribution with interference of 0.5 mm and fluid pressure of 52 MPa; (f) diagram of stress distribution when the interference amount is 0.75 mm and the fluid pressure is 35 MPa; (g) diagram of stress distribution with interference of 0.75 mm and fluid pressure of 52 MPa.

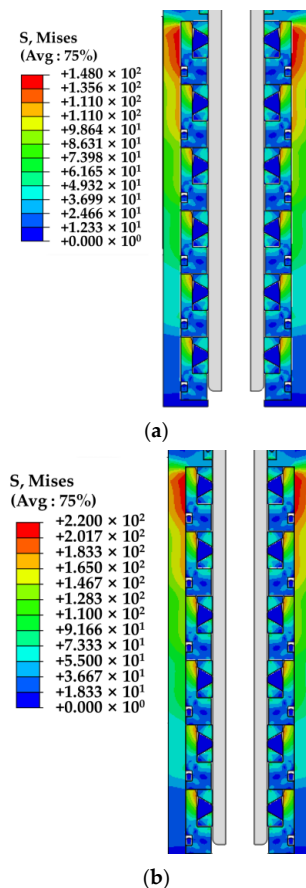


Figure 11. Cont.

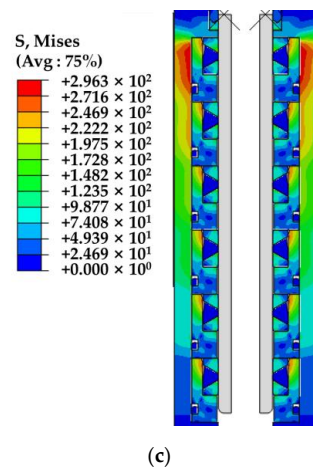


Figure 11. von Mises stress nephogram of rubber barrel at different flow pressure with a radius of 18.8 mm: (a) the fluid pressure is 35 MPa; (b) the fluid pressure is 52 MPa; (c) the fluid pressure is 70 MPa.

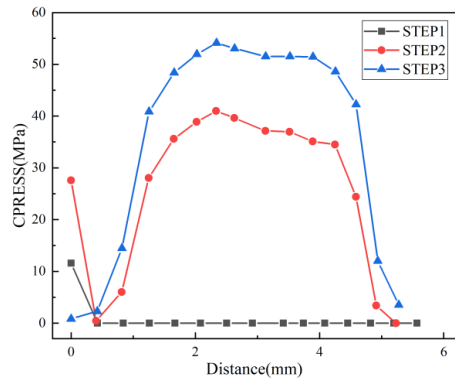
Table 2. Variation of the maximum von Mises stress under different fluid pressures and different amounts of interference.

Interference (mm)	Maximum von Mises Stress (MPa)		
	35	52	70
0.25	29.65	30.87	32.47
0.5	31.64	32.35	—
0.75	36.44	37.50	—

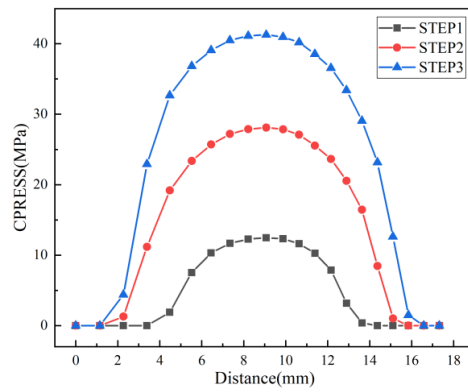
It can be seen from Table 2 that the maximum von Mises stress increases at a high rate with the increase in interference. From the process optimization perspective, the maximum von Mises stress should be less sensitive to the geometric parameters of interference. The stress variation under different fluid pressures can be obtained. With the increase in fluid pressure, the stress relaxation rate increased significantly. von Mises stress is greatly affected by the amount of interference; with the increase in relaxation range, the reliability of the sealing ring decreases.

It can be seen from Figure 12 that, without fluid pressure, the contact pressure distribution presents a quadratic curve, and is symmetrical from the maximum point to both sides. At the same time, the maximum contact pressure increases with the increase in the interference amount, which is very beneficial to the sealing effect. When the fluid pressure is 70 MPa, the maximum contact pressure of the sealing surface is always greater than the fluid pressure. The contact pressure of the O sealing ring is always more significant than fluid pressure. The above findings indicate that the triangular and O-ring seals perform well.

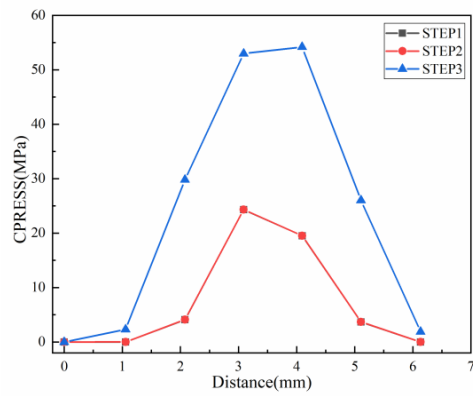
- (1) Under the condition of a certain amount of interference, the von Mises stress of the triangular seal increases with fluid pressure. It can be seen from Figure 12 that the peak position of von Mises stress also changes with the fluid pressure, indicating that the position where the seal may crack changes with the increase in fluid pressure.
- (2) Under the constant fluid pressure, with the increase in interference difference, the maximum von Mises stress increases rapidly, the material “stiffness” decreases, and the risk of cracking increases, thus negatively affecting sealing performance and sealing failure. Therefore, the size of the sealing ring should be adjusted appropriately to ensure the seal’s reliability.
- (3) The maximum contact pressure between the triangular seal and the smooth rod increases with interference and fluid pressure. The maximum contact pressure determines the sealing effect of the triangular seal. Under different high pressures, the maximum contact pressure is always greater than the fluid pressure, which meets the sealing condition and ensures the sealing function of the tool.



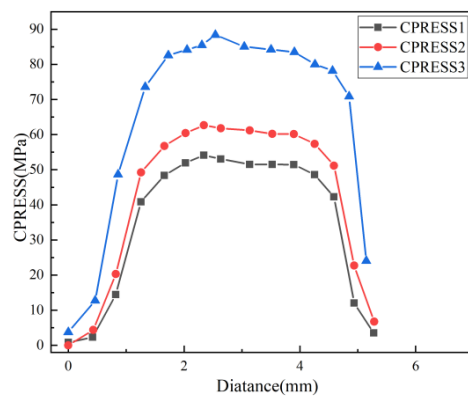
(a)



(b)

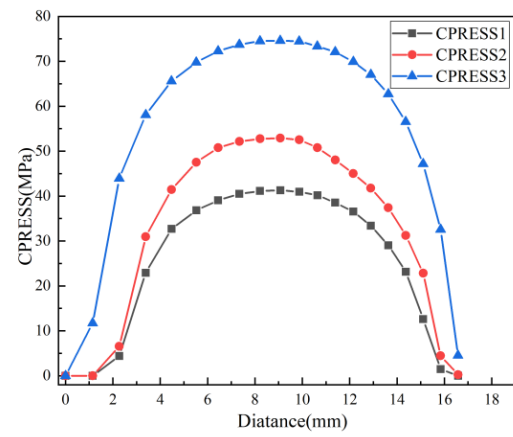


(c)

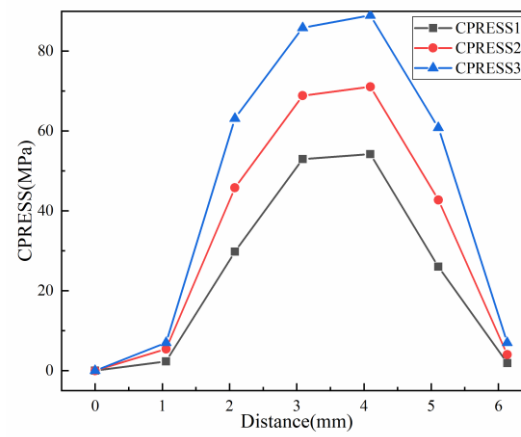


(d)

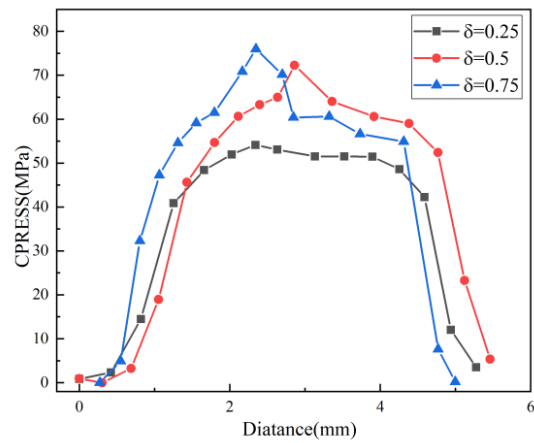
Figure 12. Cont.



(e)

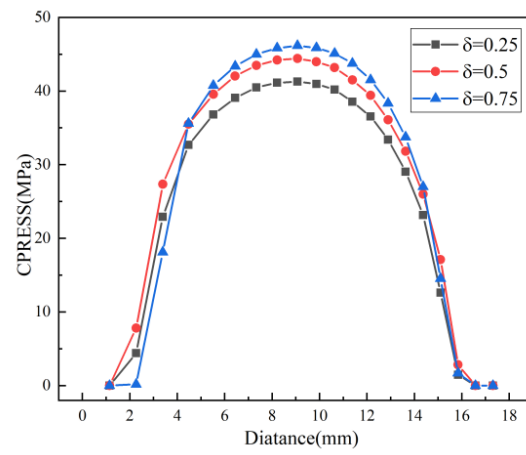


(f)

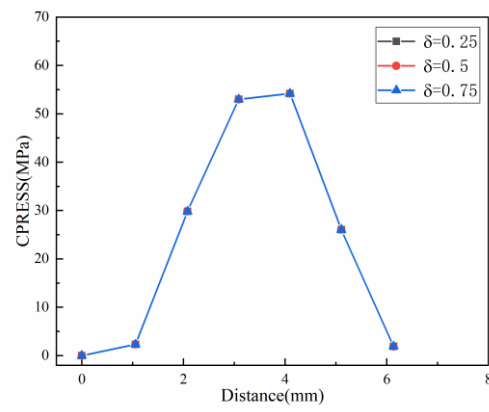


(g)

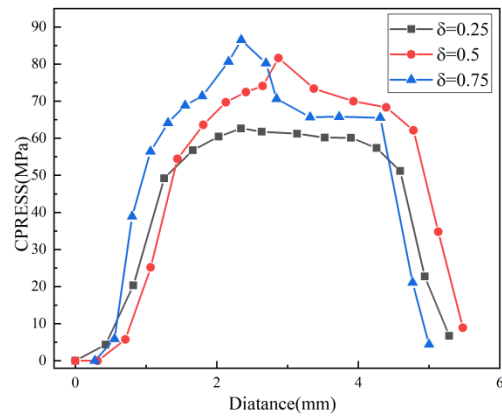
Figure 12. Cont.



(h)

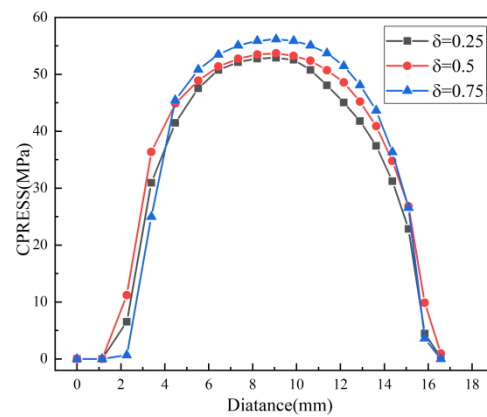


(i)

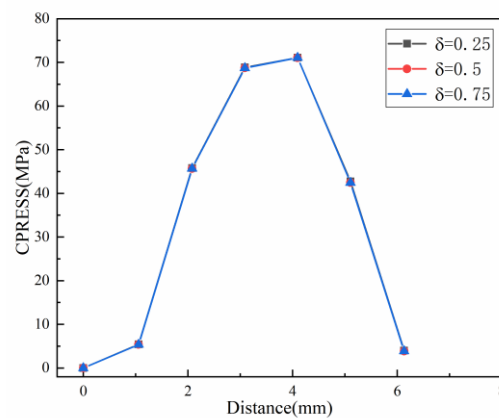


(j)

Figure 12. Cont.



(k)



(l)

Figure 12. Contact pressure. (a–c) The interference amount (δ) is 0.25 mm, the fluid pressure is 35 MPa, and the contact pressure at the rubber head, rubber bottom, and O-ring obtained at different analysis steps. (d–f) The interference amount (δ) is 0.25 mm, the fluid pressure is 35 MPa, 52 MPa, 70 MPa, and the comparison of the contact pressure at the rubber head, rubber sole, and O-ring. (g–i) The comparison of contact pressure of rubber head, rubber sole, and O-ring when the interference amount (δ) is 0.25 mm, 0.5 mm, and 0.75 mm, and the fluid pressure is 35 MPa. (j–l) The comparison of contact pressure of rubber head, rubber sole, and O-ring when the interference amount (δ) is 0.25 mm, 0.5 mm, and 0.75 mm, and the fluid pressure is 52 MPa.

4. Dynamic Seal Test

4.1. Experimental Device

A laboratory test bench was built to test the high-pressure sealing performance of the sealing tool. The dynamic seal laboratory test device is shown in Figure 13. It mainly comprises a hydraulic power cylinder, a smooth rod, a dynamic seal assembly, a heating device (Figure 14), a pressurization system, and a test bench. The soft rod was sandblasted to increase its surface roughness. The device can provide an accurate drawing, temperature, and pressure environment for the experiment. At the same time, it was equipped with pressure, temperature, and force sensors, as well as leakage collection and measurement devices to monitor and record the whole experiment process in real time. Experiments were carried out on the sealing performance of dynamic seal assembly, the abrasion resistance of dynamic seal components (as shown in area A), the movement resistance of dynamic seal assembly under pressure (as shown in area B), the sealing performance of dynamic seal assembly at 150 °C (as shown in area C), and movement resistance of dynamic seal assembly under pressure at 150 °C (as shown in area D). Combined with the simulation

data and test results, the continuous sucker rod dynamic sealing tool was modified to provide theoretical guidance for practical application.

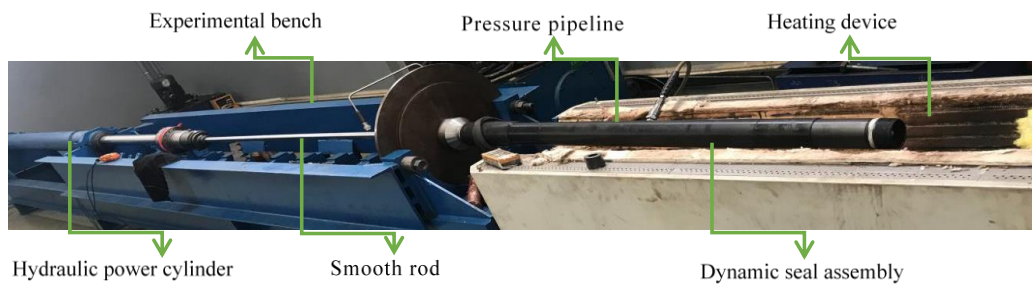


Figure 13. Experimental device.

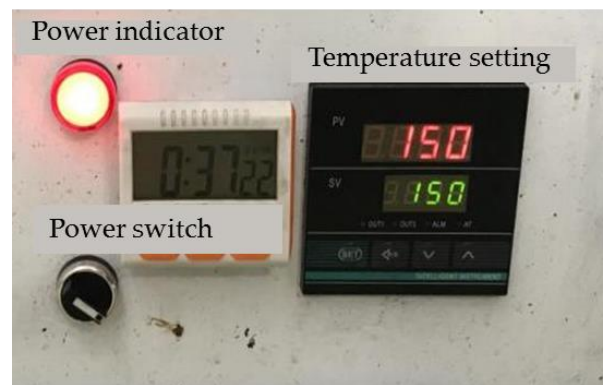


Figure 14. Temperature control box (Suzhou Honghe electric heating equipment Co., Ltd, Suzhou, China).

A test hole was set up between two dynamic sealing assembly sealing groups (Figure 15). First, the rod passed through it. Then, hydraulic pressure was drilled from the test hole to verify the pressure-bearing capacity of the static seal. The pressure was 36.3 MPa and 35.3 MPa after stabilization. After 15 min, the pressure decreased by 0.1 MPa to 35.2 MPa. There was no liquid leakage at both ends of the dynamic seal, which indicated that the sealing effect of the tool was reasonable under the static seal state.

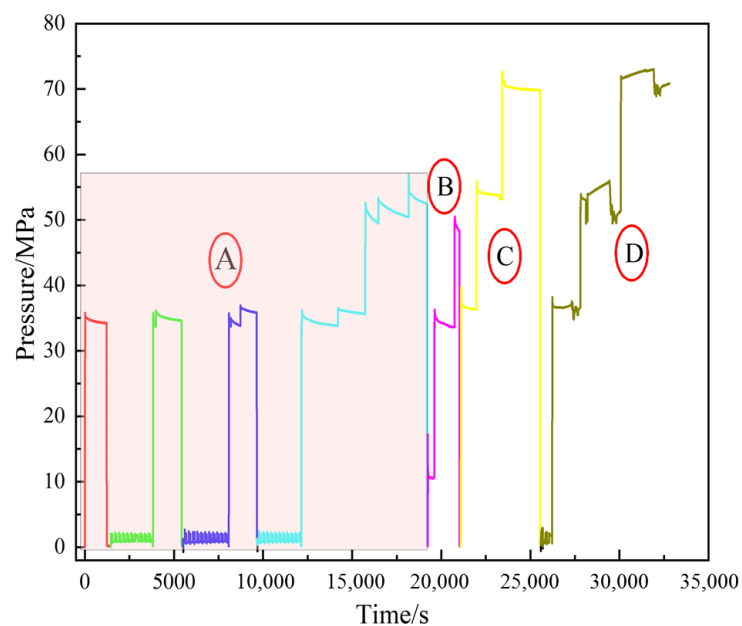


Figure 15. Pressure change curve of dynamic seal assembly pressure test.

4.2. Wear Resistance Test

The sealing performance of the dynamic seal was evaluated after passing a coiled tubing with a length of 153 m, and the wear resistance of push–pull pressing was tested. A back-and-forth stroke of the hydraulic cylinder was 3 m. After 20, 30, 40, and 51 times of push–pull, the movement performance of the dynamic seal assembly was tested under pressure (as shown in Figure 16). After 20 times of push–pull, the cumulative stroke was 60 m, and the push-and-pull load was 0.5–0.9 tons. After stabilizing hydraulic pressure, the pressure in the working cavity was 34.6 MPa. After holding the pressure for 15 min, the pressure was 34.3 MPa, with a pressure drop of 0.3 MPa (as shown in Area ①). There was no liquid leakage at both ends of the dynamic seal. After 30 times of push–pull, the cumulative stroke was 90 m, and the push-and-pull load was 0.5–0.6 tons (as shown in Area ②). After the stabilization of hydraulic pressure, the pressure was 35.2 MPa. After holding the pressure for 15 min, the pressure was 34.7 MPa and the pressure drop was 0.5 MPa (as shown in Area ③). There was no liquid leakage at both ends of the dynamic seal. After 40 times of push–pull, the cumulative stroke was 120 m, and the push-and-pull load was 0.5–0.8 tons (as shown in Area ④). After the stabilization of hydraulic pressure, the pressure was 36.3 MPa. After the pressure was maintained for 10 min, the pressure was 35.9 MPa and the pressure drop was 0.4 MPa (as shown in Area ⑤). There was no liquid leakage at both ends of the dynamic seal. After 51 times of push–pull, the cumulative stroke was 153 m, and the push-and-pull load was 0.5–0.6 tons (as shown in Area ⑥). After stabilizing hydraulic pressure, the pressure was 36 MPa and 34.6 MPa with a pressure drop of 0.4 MPa after holding the pressure for 15 min. There was no liquid leakage at both ends of the dynamic seal. The pressure continued rising to 52 MPa and then stabilized for 15 min. The pressure drop was within a small range (as shown in Area ⑦). Visual inspection showed no liquid leakage at both ends of the dynamic seal. The pressure drop was largely attributed to the cavity’s too-small volume and the liquid’s presence in the liquid inlet hole and the pressure pipeline. The minor deformation of the pipeline and the seals resulted in the fluctuation of the pressure curve. The high-pressure sealing ability was maintained after lots of push–pull, suggesting that the dynamic sealing component has qualified wear resistance. However, in the actual construction process, sharp spines or debris on the tube surface may damage the integrity of the rubber material, leading to high-pressure water leakage.

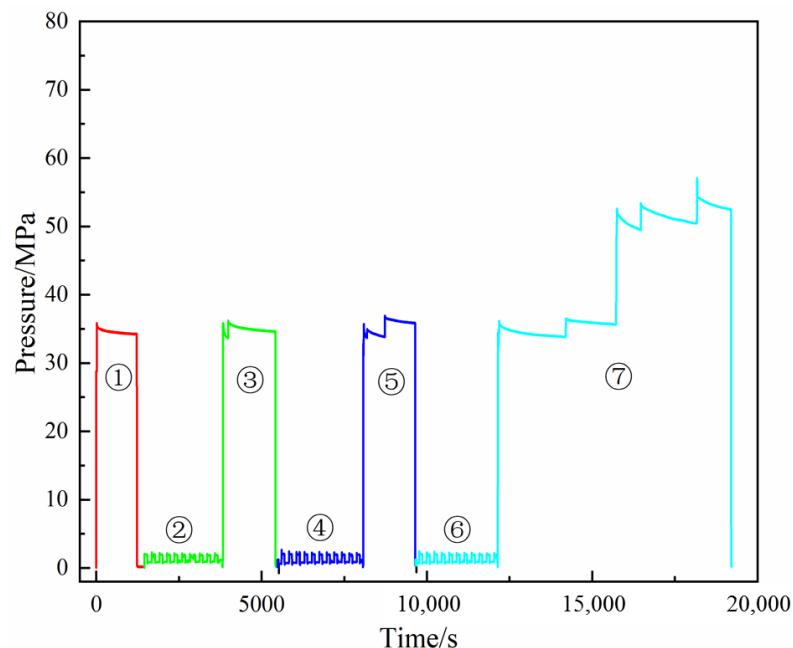


Figure 16. Wear resistance test of push–pull pressure.

4.3. Movement Resistance Test with Pressure

The distribution and coupling of the two were designed to simulate the actual working conditions of pressure and temperature. Figure 17 is the sealing pressure and push–pull load curve under the pressure of the dynamic seal assembly. As can be seen from the figure, different seal pressures (10.67 MPa, 35.13 MPa, and 49.65 MPa) had no significant effect on the push–pull force. On the contrary, the reciprocating movement of the rod did not lead to a change in the sealing pressure, which implied that the dynamic sealing structure met the sealing and sliding requirements between the formation pipe and the oil pipe below 50 MPa.

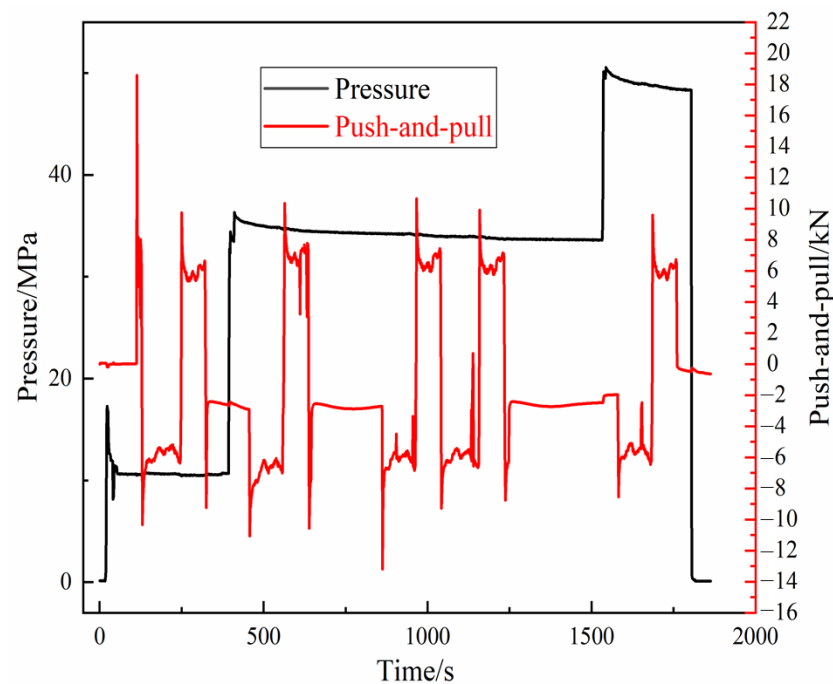


Figure 17. Test seal pressure and push–pull load curve with pressure.

4.4. High-Temperature Pressure Seal Test

The construction stratum of the sealing tool was characterized by depth, high temperature, and high pressure. Figure 18 shows the pressure sealing test of the dynamic sealing assembly under the sealing pressure of 37 MPa, 53 MPa, and 72 MPa at a high temperature of 150 °C. After being stabilized for 15 min the pressure increased by 0.2 MPa, 1.7 MPa, and 1.2 MPa, respectively, and there was no liquid leakage at both ends of the dynamic seal. The increased pressure in the process of pressure stabilization was caused by temperature fluctuation, without any pressure drop or liquid leakage in the experimental process, which indicated that the device demonstrated good sealing performance.

4.5. Movement Resistance Test with Temperate Pressure

The movement resistance test with temperate pressure is a comprehensive test of the above contents. Figure 19 shows the push–pull experimental records under 37 MPa, 53 MPa, and 72 MPa sealing pressures in a high-temperature environment of 150 °C. The movement resistance experiment was carried out at 150 °C and 37 MPa. The first thrust was 0.62–0.92 t, and the tension was 0.75–1.05 t. The second thrust was 0.4–0.72 t, and the tension was 0.6–0.8 t, during which the pressure fluctuated from 37.4 MPa to 34.9 MPa. Keeping the temperature unchanged, the pressure was increased to 53 MPa, the first thrust was 0.95–1.15 t and the tension was 0.81–1.12 t. The second thrust was 0.82–0.95 t, and the tension was 1.34–1.65 t, during which the pressure fluctuated from 56 MPa to 49.4 MPa. If the pressure continued to be increased to 72 MPa, the first thrust was 1.27–1.35 t, and the tension was 1.2–1.45 t. The second thrust was 1.2–1.38 t and the tension was 1.0–1.9 t,

during which the pressure fluctuated from 72.85 MPa to 68.72 MPa. It can be seen from the figure that temperature resulted in a significant increase in push–pull force (about 2–5 kN). With the increase in sealing pressure, the push–pull force increased slightly. At the same time, a minor fluctuation in the sealing pressure was observed in the push–pull process, accompanied by a small amount of leakage, as shown in Figure 20. The results show that the pressure is still stable at a certain value after push–pull, verifying the reliability of the sealing tool under high-temperature and high-pressure environments.

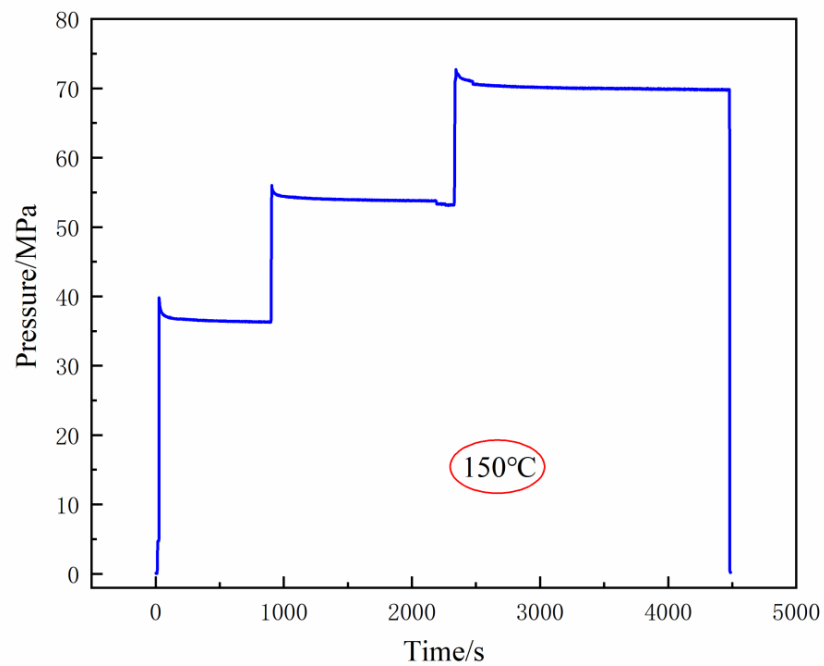


Figure 18. Test pressure curve of high-temperature pressure seal.

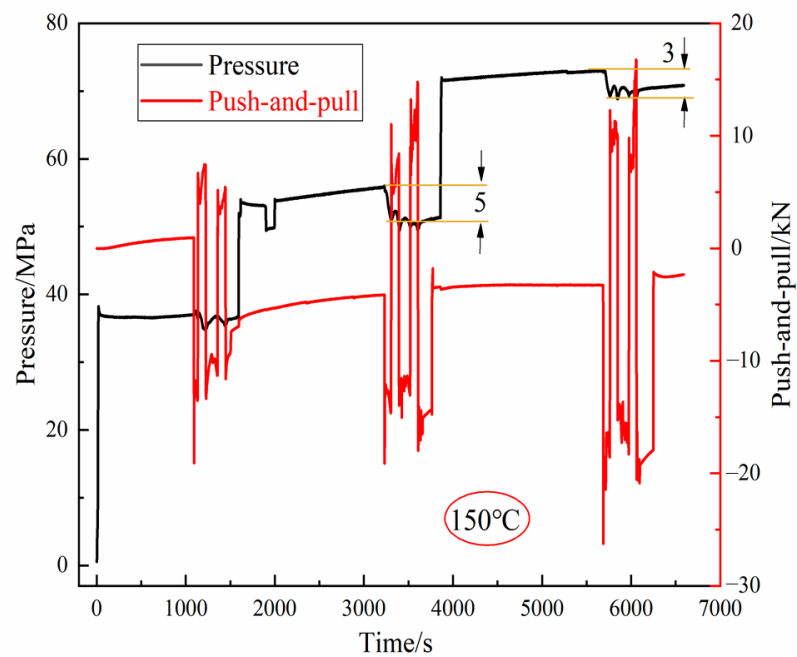


Figure 19. Sealing pressure and push–pull force changes during reciprocating motion with pressure and temperature.



Figure 20. Check the leakage device.

In addition, it can be seen from Figure 21 that the triangular sealing ring is the main wear part. The middle of the inner lip suffers the most severe wear, which is consistent with the position of the maximum contact pressure simulation result, further confirming the accuracy of the numerical simulation.



Figure 21. Triangular seal wear.

5. Conclusions

The test results of the smooth rod entry seal under different seal pressures, seal performance of dynamic seal assembly, wear resistance of dynamic seal assembly, and motion resistance of dynamic seal with pressure show that the sealing performance of dynamic seal meets the design requirements without any liquid leakage. The performance test of a push-pull seal with pressure at 150 °C shows that the construction of the sealing tool is affected by temperature. A minor fluctuation in the sealing pressure can be seen in the push-pull process, accompanied by a small amount of leakage, resulting in reduced but stable pressure after push-pull, verifying the sealing performance of the sealing tool under high temperature and pressure. The tool meets the requirements of the Tahe ultra-deep

carbonate construction environment and realizes the connection of the fracture–cavity carbonate reservoir.

The simulation results show that the maximum contact pressure under working conditions increases with fluid pressure, and the sealing condition is always satisfied. Under the action of 70 MPa of high-pressure fluid, the von Mises stress of the sealing ring is 32.47 MPa, which is within a reasonable range. However, the size of the triangular sealing ring dramatically affects the life of the sealing tool. The stress concentration occurs in the inner lip area between the triangular sealing ring and the smooth rod. Too much interference will relax the sealing ring's stress and reduce its elasticity, finally leading to permanent deformation, reducing the service life of the sealing ring, and then making it lose its ability to seal. The size of the sealing ring should be reasonably selected according to the actual construction requirements. Furthermore, as the surface finish of the smooth rod in the ground experiment is much better than that of the continuous oil tubing in the field, the results of this test may not reflect the actual wear of the seal assembly. It is recommended that sections of the coiled tubing be polished prior to drilling through the mobile seal assembly to minimize surface damage to the rubber seal. To sum up, the structural design of the moving seal assembly is reasonable, and the combination of multiple triangular seals can solve the problem of high-pressure tightness.

Author Contributions: Conceptualization, L.C. and Y.L.; methodology, Y.L.; software, L.C.; validation, L.C. and W.G.; formal analysis, L.C.; investigation, L.C.; resources, Y.L.; data curation, G.C.; writing—original draft preparation, L.C.; writing—review and editing, L.C.; visualization, Y.L. and Z.D.; supervision, Y.L.; project administration, Y.L. and Q.S.; funding acquisition, Y.L. All authors have read and agreed to the published version of the manuscript.

Funding: The authors gratefully acknowledge the financial support from the National Key Research and Development Program of China (Grant No. 2023YFF0615403), the Young Elite Scientist Sponsorship Program by CAST (No. YESS20220404), the Scientific Research and Technology Development Project of CNPC (Grant No. 2021DJ4601) and Fundamental Research Funds for the Central Universities, China (No. 379202408).

Data Availability Statement: The raw data supporting the conclusions of this article will be made available by the authors upon request.

Conflicts of Interest: Authors Lin Chai and Qiang Sun were employed by the company CNPC. Author Wenlong Gao was employed by the company China National Petroleum Corporation Great Wall Drilling Engineering Co., Ltd. The remaining authors declare that the research was conducted in the absence of any commercial or financial relationships that could be construed as a potential conflict of interest. The [companies CNPC and China National Petroleum Corporation Great Wall Drilling Engineering Co., Ltd. in affiliation] had no role in the design of the study; in the collection, analyses, or interpretation of data; in the writing of the manuscript, or in the decision to publish the results.

References

1. Deng, L.; Li, W.; Shu, C.X.; Xing, Z. Drilling depth analysis of hydraulic jet radial horizontal well. *Sci. J. Intell. Syst. Res.* **2021**, *3*, 31–45.
2. Wang, B.; Gensheng, L.; Zhongwei, H.; Jingbin, L.; Dongbo, Z.; Hao, L. Hydraulics calculations and field application of radial jet drilling. *SPE Drill. Complet.* **2000**, *31*, 71–81.
3. Huang, Z. Review of radial jet drilling and the key issues to be applied in new geo-energy exploitation. *Energy Procedia* **2019**, *158*, 5969–5974. [[CrossRef](#)]
4. Dickinson, W.; Anderson, R.R.; Dickinson, R.W. The ultrashort-radius radial system. *SPE Drill. Eng.* **1989**, *4*, 247–254. [[CrossRef](#)]
5. Zhang, S.; Hu, Y.; Li, G.; Tan, W.; Li, J.; Gao, Z.; Zhang, Z. Radial drilling and fracturing technology for short horizontal section of coalbed methane and its application. *Coal Sci. Technol.* **2016**, *44*, 50–53.
6. Zhang, Q.; Liu, H.; Kang, X.; Liu, Y.; Dong, X.; Wang, Y.; Liu, S.; Li, G. An investigation of production performance by cyclic steam stimulation using horizontal well in heavy oil reservoirs. *Energy* **2021**, *218*, 119500. [[CrossRef](#)]
7. Dong, Y.; Xu, A.Z. Application of the imitation horizontal well technique in the development of low permeability reservoirs. *Adv. Mater. Res.* **2013**, *734–737*, 1350–1353.
8. Cai, W.B.; Li, Z.M.; Zhang, X.L.; Zhang, B.; Zhang, Q. Horizontal well fracturing technology for reservoirs with low permeability. *Pet. Explor. Dev. Online* **2009**, *36*, 80–85.

9. Xu, Y.; Li, X.; Liu, Q.; Tan, X. Pressure performance of multi-stage fractured horizontal well considering stress sensitivity and dual permeability in fractured gas reservoirs. *J. Pet. Sci. Eng.* **2021**, *201*, 108154. [[CrossRef](#)]
10. Best, D.A.; Cordell, G.M.; Hastonm, J.A. Underground test facility: Shaft/Tunnel Labo, ratory for horizontal well technology. *J. Pet. Technol.* **1987**, *39*, 603–612. [[CrossRef](#)]
11. Zhang, W.; Duan, T.; Li, M.; Zhao, H.; Shang, X.; Wang, Y. Architecture characterization of ordovician fault-controlled paleokarst carbonate reservoirs in Tuoputai, Tahe oilfield, Tarim Basin, NW China. *Pet. Explor. Dev.* **2021**, *48*, 367–380. [[CrossRef](#)]
12. Zheng, S.; Yang, M.; Kang, Z.; Liu, Z.; Long, X.; Liu, K.; Li, X.; Zhang, S. Controlling factors of remaining oil distribution after water flooding and enhanced oil recovery methods for fracture-cavity carbonate reservoirs in Tahe Oilfield. *Pet. Explor. Dev.* **2019**, *46*, 786–795. [[CrossRef](#)]
13. Ding, Z.; Wang, R.; Chen, F.; Yang, J.; Zhu, Z.; Yang, Z.; Sun, X.; Xian, B.; Li, E.; Shi, T.; et al. Origin, hydrocarbon accumulation and oil-gas enrichment of fault-karst carbonate reservoirs: A case study of Ordovician carbonate reservoirs in South Tahe area of Halahatang oilfield, Tarim Basin. *Pet. Explor. Dev.* **2020**, *47*, 306–317. [[CrossRef](#)]
14. Qin, G.H.; Gao, X.S.; Yan, Z.L. Analysis of thermal recovery horizontal well drilling technology in Gudong Nine District. *Adv. Pet. Explor. Dev.* **2015**, *1*, 111–114.
15. Tian, S.; Huang, Z.; Li, G.; Lu, P.; Zhang, H.; Wang, T. Laboratory experiments on blockage removing and stimulation of CBM reservoirs by composite pulsating hydraulic fracturing of radial horizontal wells. *Nat. Gas Ind. B* **2019**, *6*, 151–158. [[CrossRef](#)]
16. Sun, J. Optimization design of self-propelled hydraulic jet bit for coalbed methane. *Int. Core J. Eng.* **2020**, *3*, 46–52.
17. Fan, S.; Li, Y.X.; Cao, J.Q.; Xie, J.B. Optimization technique in double stepped thin horizontal well. *Adv. Mater. Res.* **2013**, *734–737*, 1226–1229.
18. Jun, Y.; Mingyue, C.; Anle, H.; Weidong, J.; Chong, L. Study and application of hydraulic jet radial drilling in Carbonate Reservoirs. *Int. J. Oil Gas Coal Eng.* **2018**, *6*, 96. [[CrossRef](#)]
19. Deshpande, K.; Mirasdar, S.P.; Mhaskar, N.A.; Joshi, R.P. Composite frac plug design optimization for efficient hydraulic fracturing operations. In Proceedings of the SPE Eastern Regional Meeting, Charleston, WV, USA, 15–17 October 2019.
20. Zhou, Z.; Kanglei, Z.; Jing, L. Finite element analysis of stress and contact pressure of O-ring. *Lubr. Seal.* **2006**, *4*, 86–89.
21. Jung, J.K.; Kim, I.G.; Kim, K.T.; Ryu, K.S.; Chung, K.S. Evaluation techniques of hydrogen permeation in sealing rubber materials. *Polym. Test.* **2021**, *93*, 107016. [[CrossRef](#)]
22. Zhou, C.; Chen, G.; Liu, P. Finite element analysis of sealing performance of rubber D-ring seal in high-pressure hydrogen storage vessel. *J. Fail. Anal. Prev.* **2018**, *18*, 846–855. [[CrossRef](#)]
23. Huang, Y.; Li, Y.; Zhao, H.; Wen, H. Research on constitutive models of hydrogenated nitrile butadiene rubber for packer at different temperatures. *J. Mech. Sci. Technol.* **2020**, *34*, 155–164. [[CrossRef](#)]
24. Hu, G.; Zhang, P.; Wang, G.; Zhang, M.; Li, M. The influence of rubber material on sealing performance of packing element in compression packer. *J. Nat. Gas Sci. Eng.* **2017**, *38*, 120–138. [[CrossRef](#)]
25. Huang, P.; Wang, Y.S.; Li, Y.; Tao, J.Y. Analysis of low temperature compression characteristics of rubber seal strip of shelter based on ABAQUS. IOP conference series. *Mater. Sci. Eng.* **2021**, *1043*, 32050.
26. Zhou, S.M.; Chen, P.; Shi, Y. Analysis on sealing performance for a new type of rubber saddle-shaped sealing ring based on AQAQUS. *Procedia Eng.* **2015**, *130*, 1000–1009. [[CrossRef](#)]
27. Zhu, J.; Zou, L.Q.; Han, S.J. The modeling of rubber sealing ring of fluid dynamic pressure and finite element analysis about stress based on SolidWorks and ANSYS. *Appl. Mech. Mater.* **2012**, *215–216*, 1246–1249.
28. Zheng, C.; Zheng, X.; Qin, J.; Liu, P.; Aibaibu, A.; Liu, Y. Nonlinear finite element analysis on the sealing performance of rubber packer for hydraulic fracturing. *J. Nat. Gas Sci. Eng.* **2021**, *85*, 103711. [[CrossRef](#)]
29. Lee, B.S.; Rivin, E.I. Finite element analysis of load-deflection and creep characteristics of compressed rubber components for vibration control devices. *J. Mech. Des.* **1996**, *3*, 328–336. [[CrossRef](#)]
30. Yi, T.; Weng, X.; Zhu, S. Static performance analysis of incompressible rubber body. *J. Nav. Univ. Eng.* **2002**, *1*, 76–80.
31. Abdelal, G.F.; Robotham, A.; Carragher, P. Numerical simulation of a patent technology for sealing of deep-sea oil wells using nonlinear finite element method. *J. Pet. Sci. Eng.* **2015**, *133*, 192–200. [[CrossRef](#)]
32. Kim, C.; Shim, W. Analysis of contact force and thermal behaviour of lip seals. *Tribol. Int.* **1997**, *2*, 113–119.
33. Chen, T.; Ma, W.; Liu, S.; Wu, J. Analysis on mechanical influencing factors of fatigue behavior for the packer on pipe ram in snubbing unit. *Eng. Fail. Anal.* **2019**, *103*, 20–31. [[CrossRef](#)]
34. Zhang, F.; Shui, H.; Yang, J. Sealing performance and fatigue life of the fracturing packer rubber of various materials. *Proc. Inst. Mech. Eng. Part C J. Mech. Eng. Sci.* **2019**, *233*, 6157–6166. [[CrossRef](#)]
35. Dong, L.; Li, K.; Zhu, X.; Li, Z.; Zhang, D.; Pan, Y.; Chen, X. Study on high temperature sealing behavior of packer rubber tube based on thermal aging experiments. *Eng. Fail. Anal.* **2020**, *108*, 104321. [[CrossRef](#)]
36. Liu, Y.; Lian, Z. Failure analysis on rubber sealing structure of mandrel hanger and improvement in extreme environments. *Eng. Fail. Anal.* **2021**, *125*, 105433. [[CrossRef](#)]

Disclaimer/Publisher’s Note: The statements, opinions and data contained in all publications are solely those of the individual author(s) and contributor(s) and not of MDPI and/or the editor(s). MDPI and/or the editor(s) disclaim responsibility for any injury to people or property resulting from any ideas, methods, instructions or products referred to in the content.